
This item was submitted to [Loughborough's Research Repository](#) by the author.
Items in Figshare are protected by copyright, with all rights reserved, unless otherwise indicated.

Pacific seamount volcanism in space and time

PLEASE CITE THE PUBLISHED VERSION

<http://dx.doi.org/10.1111/j.1365-246X.2006.03250.x>

PUBLISHER

© The Author Journal compilation © RAS

VERSION

VoR (Version of Record)

LICENCE

CC BY-NC-ND 4.0

REPOSITORY RECORD

Hillier, John K.. 2019. "Pacific Seamount Volcanism in Space and Time". figshare.
<https://hdl.handle.net/2134/13045>.

This item was submitted to Loughborough's Institutional Repository (<https://dspace.lboro.ac.uk/>) by the author and is made available under the following Creative Commons Licence conditions.



CC creative commons
COMMONS DEED

Attribution-NonCommercial-NoDerivs 2.5

You are free:

- to copy, distribute, display, and perform the work

Under the following conditions:

 **Attribution.** You must attribute the work in the manner specified by the author or licensor.

 **Noncommercial.** You may not use this work for commercial purposes.

 **No Derivative Works.** You may not alter, transform, or build upon this work.

- For any reuse or distribution, you must make clear to others the license terms of this work.
- Any of these conditions can be waived if you get permission from the copyright holder.

Your fair use and other rights are in no way affected by the above.

This is a human-readable summary of the [Legal Code \(the full license\)](#).

[Disclaimer](#) 

For the full text of this licence, please go to:
<http://creativecommons.org/licenses/by-nc-nd/2.5/>

Pacific seamount volcanism in space and time

J. K. Hillier

Department of Earth Sciences, University of Cambridge, Downing Street, Cambridge CB2 3EQ, UK. E-mail: jkh34@cam.ac.uk

Accepted 2006 September 27. Received 2006 June 29; in original form 2005 November 20

SUMMARY

Seamounts constitute some of the most direct evidence about intraplate volcanism. As such, when seamounts formed and into which tectonic setting they erupted (i.e. on-ridge or off-ridge) are a useful reflection of how the properties of the lithosphere interact with magma generation in the fluid mantle beneath. Proportionately few seamounts are radiometrically dated however, and these tend to be recently active.

In order to more representatively sample and better understand Pacific seamount volcanism this paper estimates the eruption ages (t_{volc}) of 2706 volcanoes via automated estimates of lithospheric strength. Lithospheric strength (GTR_{rel}) is deduced from the ratio of gravity to topography above the summits of volcanoes, and is shown to correlate with seafloor age at the time of volcanic loading (Δt) at 61 sites where radiometric constraints upon Δt exist. A trend of $GTR_{\text{rel}} = 0.09825\sqrt{\Delta t} + 0.20251$ fits data for these 61, and with seafloor age (t_{sf}) known, can date the 2706 volcanoes; $t_{\text{volc}} = t_{\text{sf}} - \Delta t$.

Widespread recurrences of volcanism proximal to older features (e.g. the Cook-Austral alignment in French Polynesia) suggest that the lithosphere exerts a significant element of control upon the location of volcanism, and that magmatic throughput leaves the lithosphere more susceptible to the passage of future melts. Observations also prompt speculation that: the Tavera seamounts share morphological characteristics and isostatic compensation state with the Musicians, and probably formed similarly; the Easter Island chain may be a modern analogy to the Cross-Lines; a Musicians – South Hawaiian seamounts alignment may be deflecting the Hawaiian hotspot trace.

Key words: flexural isostasy, lithosphere, pacific, seamount dating, volcanism.

1 INTRODUCTION

Beneath the world's oceans, the seafloor is littered with relatively small-scale (up to ~ 250 km across) rises that are subcircular in plan view. By analogy with volcanic oceanic islands, and by direct sampling of a few hundred (i.e. < 1 per cent; Wessel 1997), these submarine mountains or 'seamounts' are thought to be volcanic. They constitute some of the most direct evidence about geodynamic processes in and below the lithosphere that control intraplate volcanism.

Dating is a critical part of this evidence. For instance, the 'hotspot' hypothesis (Wilson 1963b; Morgan 1971), where linear volcanic chains on a moving tectonic plate may be traced back to a single approximately stationary region of high magma productivity, seeks to explain edifices of monotonically increasing age to the NW along the Hawaiian-Emperor seamount chain.

Up to 50 000 seamounts taller than 1 km are estimated to exist in the Pacific (Menard 1964; Wessel & Lyons 1997), 12 000 of which have been counted on maps (Batiza 1982). Unfortunately, only ~ 250 are radiometrically dated after direct sampling (Fig. 1), and these

samples favour recent hotspot volcanism (39 per cent of ages are < 10 Ma, 3.8 times greater than in any other 10 Ma interval), so the distribution of seamount volcanism in space and time is not representatively sampled.

An alternative, albeit indirect, technique to constrain seamount ages uses an elastic plate model of regional isostatic compensation to reconcile the relationship between gravity and bathymetry. The plate rigidity required (commonly quantified as plate thickness, T_e) systematically increases with lithospheric age at the time of loading, Δt (Watts 1978; Watts *et al.* 1980; Calmant *et al.* 1990; Watts 2001). Since lithospheric age in the proximity of a seamount, t_{sf} , is relatively well dated by magnetic lineations in the ridge-produced oceanic crust, rigidity can be related to Δt and edifice age, t_{volc} ; $t_{\text{volc}} = t_{\text{sf}} - \Delta t$.

Watts *et al.* (1980) constrained the tectonic setting of volcanic emplacement for ~ 130 seamounts to be 'on-ridge' (Δt 2–8 Ma) or 'off-ridge' ($\Delta t > 35$ Ma). Craig & Sandwell (1988) estimated rigidity from nine Seasat altimeter profiles. Calmant *et al.* (1990) first proposed quantitatively inverting the relationship between rigidity and Δt , fitting $T_e = 2.7 \pm 0.15\sqrt{\Delta t}$ to 36 data, but only dating the

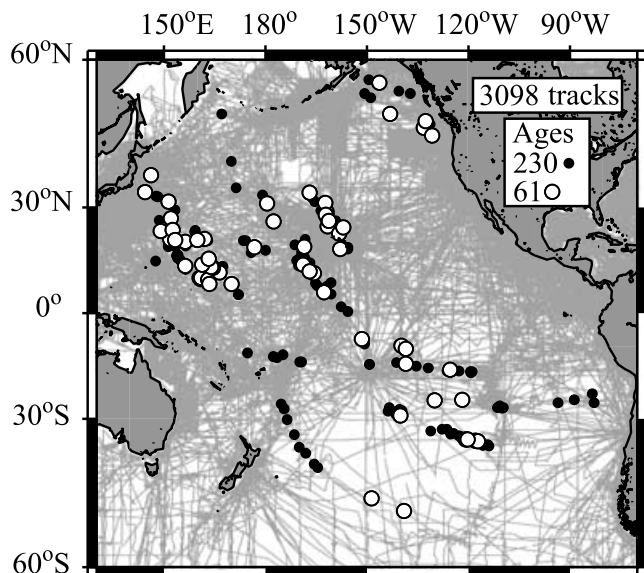


Figure 1. Locations of data sets. Grey lines are echo-sounder data, mainly from the GEODAS database (NOAA 2003). 230 black dots are better quality radiometric dates from seamounts: Koppers *et al.* (2003) supplemented by Clouard & Bonneville (2005). 61 white circles overlie some of these where there are also geophysical strength estimates in this study (see Section 2.3).

Trinidad Chain. Wessel (1997) calculated 8022 ‘pseudo-ages’ from gravity anomalies, but Wessel (2001) asserted that these were based on an unreliable assumption that all seamounts grow to a limiting height related to Δt (Epp 1984). Wessel & Lyons’ (1997) predictions of seamount height incorporated a T_e -height relationship, so Watts’ (2001) inversion of their ratios of gravity to topography (GTRs) contained circularity. Thus, such geophysical approaches have not yet been successfully applied *en masse* to date Pacific seamounts.

This paper uses the height of seamounts independently estimated from ship-track echo-sounder data, compares this to the gravity anomaly over their summits, and from this robustly measures lithospheric strength (see Hillier 2005; Hillier & Watts 2005b). A subset, 61 of 2706 strength estimates, is calibrated against radiometric measures of Δt in order to constrain self-consistently the ages and tectonic settings of all 2706 seamounts.

2 METHOD

An elastic plate model of regional (i.e. flexural) isostatic compensation (e.g. Vening Meinesz 1941; Gunn 1943; Watts & Daly 1981, Fig. 2) well reconciles the relationship between gravity and bathymetry over seamounts (e.g. Watts 1978; Freedman & Parsons 1986). With increasing plate thickness the ratio of gravity to seamount height (also called topography) above the centre of a seamount rises. G is gravity, T is topography, and the ratio the GTR. As well as lithospheric strength, however, a seamount’s GTR is affected by its height, shape and depth, which must be independently determined from bathymetry data. So, in order to estimate self-consistently volcano ages from GTRs following five steps are necessary:

- (i) Find T for seamounts.
- (ii) Measure G for as many of these as possible.
- (iii) Use GTR values to measure lithospheric strength.
- (iv) At a subset of sites where radiometric estimates of Δt exist, calibrate strength against Δt .

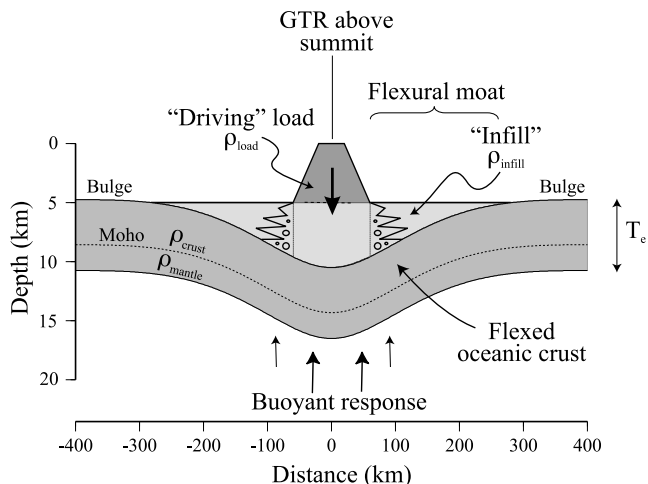


Figure 2. Thin elastic plate model as applied to an oceanic seamount, adapted from (Watts 2001). A volcano (dark grey) loads a strong lithosphere and causing a distributed depression (light grey) including a flexural moat and a bulge. The buoyancy response is created when less dense material (crust) is pushed downwards into more dense material (mantle). The effective thickness of the mechanically strong lithosphere, T_e , is the thickness of a standard plate (with properties of each author’s choosing, see Appendix B) that has a rigidity causing it to best fit the observed deformation. ρ is density, vertical arrows represent forces.

- (v) Use the calibrated relationship between strength and Δt to date the seamounts.

These are detailed in order, then the method is discussed.

2.1 Isolating seamounts’ bathymetry

To avoid the size distortions present in regularised bathymetric grids (e.g. ETOPO-5) (McNutt 1998), the dimensions of seamounts are determined directly from 21.7×10^6 km of 3098 echo-sounder profiles shown in Fig. 1. Using scale-independent morphological criteria, seamounts up to 200 km across are isolated from larger-scale trends such as hotspot swells using MiMIC, an algorithm already proven across the Pacific (Hillier & Watts 2004, 2005a). The resulting traverses across seamounts are approximated as flat-topped trapezia (e.g. Jordan *et al.* 1983; Smith 1988; Smith & Jordan 1988; Smith & Cann 1992; Bridges 1997; Hammond 1997; Rappaport *et al.* 1997; Wessel 2001) optimized using a simplex-like method (Appendix A). Only trapezia well fit in shape and cross-sectional area are retained ($\Delta_{Area} < 10$ per cent). Traverses that do not pass directly (i.e. edge₁-summit-edge₂ acute angle of $< 150^\circ$, or an along-track distance of > 110 per cent of a direct path) across seamounts are also discounted at this point. Finally, where multiple traverses of a seamount exist, the tallest trapezium is presumed to best estimate the relief of a radially symmetric seamount. 121 882 heights (> 100 m) of possible seamounts are determined, 3874 > 1.5 km high and likely to produce a distinct gravity anomaly (Wessel & Lyons 1997).

2.2 Associating seamounts with gravity anomalies

2706 of the 121 882 height determinations thought to represent seamounts are located coincident with one of Wessel & Lyons’ (1997) 7968 gravity anomalies in the area 60°S – 60°N and 130°E – 70°W ; namely, the centre of the gravity anomaly is within the bathymetric footprint of the seamount. These gravity anomalies were carefully isolated from larger-scale spatial trends in the gravity field

Table 1. Values of physical parameters.

Parameter	Value
Gravity	9.81 ms ⁻²
Young's Modulus	10 ¹¹ N m
Poisson's Ratio	0.25
Mantle density	3330 kg m ⁻³
Crustal density	2800 kg m ⁻³
Infill density	2650 kg m ⁻³
Load density	2800 kg m ⁻³
Water density	1030 kg m ⁻³
Crustal thickness	7 km

such that they most likely represented seamounts. Any disagreement in location may result from either incomplete coverage bathymetric, incomplete gravity coverage (~10 km track spacing), or migration during the gravity anomaly location procedure of Wessel & Lyons (1997). Uncertainty also exists where seamounts are in close proximity and their flanks merge substantially. Here interpretation of the two data sets may differ and, when more than one gravity anomaly falls within a bathymetric footprint, the seamount is discarded and does not contribute to the total of 2706. These GTR observations are now ready to be interpreted in terms of a flexural model, and then related to Δt values.

2.3 Estimating lithospheric strength

In theory, for each seamount, an observed GTR value (GTR_{obs}) falls somewhere on a linear scale between a minimum and a maximum theoretical GTR value (GTR_{min} & GTR_{max}) representing very strong and very weak lithosphere, respectively. The position of GTR_{obs} on the scale relative to these extreme strength values relates to the strength of the lithosphere supporting the seamount. This position may be dubbed GTR_{rel} , quantified (see eq. 1), and is a measure of lithospheric strength in the way that T_e is.

$$GTR_{rel} = \frac{GTR_{obs} - GTR_{min}}{GTR_{max} - GTR_{min}}. \quad (1)$$

Practically, for each seamount, a plate with rigidity equivalent to a T_e of 40 km is used to approximate GTR_{max} , and equivalent to a T_e of 0.01 km used for GTR_{min} . An FFT solution of the flexural equation that allows for an arbitrarily shaped load and infill density to differ from load density (p188 of Watts 2001) is computed within a 660 × 660 km area using physical constants in Table 1.

In an additional step measurement errors, estimated as ± 250 m (1 standard deviation, σ) for topography (Carter 1980; Smith 1993) and ± 5 mGal (1σ) for gravity (Neuman *et al.* 1993; Marks 1996; Smith & Sandwell 1997), are accounted for by expanding the theoretical GTR range by an amount $\pm \epsilon$, where $\epsilon = [(500 \text{ m/T}) + (10 \text{ mGal/G})] \times GTR_{obs}$; an arbitrary but simple function. 500 m and 10 mGal represent 2σ errors in topography and gravity, respectively, and T and G are still observed topography and gravity over the centre of the seamount. This amendment is implemented by replacing GTR_{min} and GTR_{max} in eq. (1) with $(GTR_{min} - \epsilon)$ and $(GTR_{max} + \epsilon)$ (see eq. 2). Using the amended form of GTR_{rel} stabilises it as a strength estimate, and is used from now on.

$$GTR_{rel} = \frac{GTR_{obs} - GTR_{min} + \epsilon}{GTR_{max} - GTR_{min} + 2\epsilon}. \quad (2)$$

It is also possible to estimate the most suitable T_e for a seamount from GTR observations if, for example, one compares GTR_{obs} to

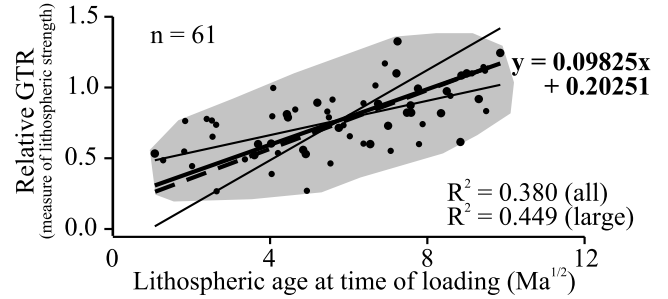


Figure 3. Scatter plot of GTR_{rel} versus independently estimated $\sqrt{\Delta t}$. GTR_{rel} is lithospheric strength at the time of volcanic loading. Δt is lithospheric age at the time of loading estimated from radiometric dating of seamounts (Koppers *et al.* 2003; Clouard & Bonneville 2005) and seafloor age the seafloor age of Müller & Roest (1997); $t_{volc} = t_{sf} - \Delta t$. Grey shading is an envelope around the data (black dots) at 61 locations (Fig. 1). Thin lines are trends fitted by the ordinary least squares method, and thick line (equation given) accounts for uncertainty in both variables (Marks & Sandwell 1991). Dashed line fits large seamounts, basal radius > 20 km, shown as bigger dots.

theoretical values of GTR computed for a spectrum of possible T_e values. Unlike for GTR_{rel} where the effect of random measurement noise remains approximately symmetrically distributed, however, T_e values are skewed to low values. T_e values, therefore, correlate substantially less strongly with radiometric estimates of Δt , and best-fitting trend lines are biased. Using GTRs, therefore, T_e is a less useful measure of strength than GTR_{rel} when dating seamounts, and GTR_{rel} is used from here on.

2.4 Calibrating strength against Δt

In order to date seamounts using geophysical estimates of lithospheric strength, it must be possible to convert strength into Δt . This can be done self-consistently within a study by taking a subset of strength data where Δt is independently 'known' and calibrating a relationship between the two.

Fig. 3 plots strength of the lithosphere at the time of volcanic loading (GTR_{rel}) against lithospheric age at the time of loading (Δt) estimated from radiometric dating of seamounts (t_{volc}) (Koppers *et al.* 2003; Clouard & Bonneville 2005) and the seafloor age (t_{sf}) of Müller & Roest (1997). The grey shading is an envelope around the data (black dots) at 61 locations (Fig. 1) where the 2706 GTR observations coincide with 'good quality' radiometric dates (Clouard & Bonneville 2005; Baksi 2005) here interpreted quite liberally as Ar/Ar dating of any sort (i.e. not K/Ar dates). This choice is arguably justified as r^2 is 0.3800 between GTR_{rel} and $\sqrt{\Delta t}$ for the selected dates, higher than an r^2 of 0.2522 for all measured dates.

Admittedly, a correlation with an r^2 of 0.3800 is not strong, but almost certainly exists: Student's t -test indicates a chance of < 1 per cent that no correlation exists. For large seamounts (basal radius > 20 km) r^2 is 0.4489. So, correlation strength is not incomparable to an r^2 of 0.4807 for a $T_e - \sqrt{\Delta t}$ compilation of local forward modelling studies by Watts (2001), and greater than an r^2 of 0.1296 for T_e versus $\sqrt{\Delta t}$ when T_e is estimated by predicting bathymetry from satellite-derived gravity for a variety of T_e values and comparing this to shipboard soundings Watts *et al.* (2006). Using the compilation of radiometric dates from Watts *et al.* (in preparation), r^2 for $GTR_{rel} - \sqrt{\Delta t}$ is 0.3861 and 0.5070 for all and large seamounts, respectively.

On Fig. 3, the trend is visible from the envelope of the data, and shown by the relatively close agreement of the best-fitting linear

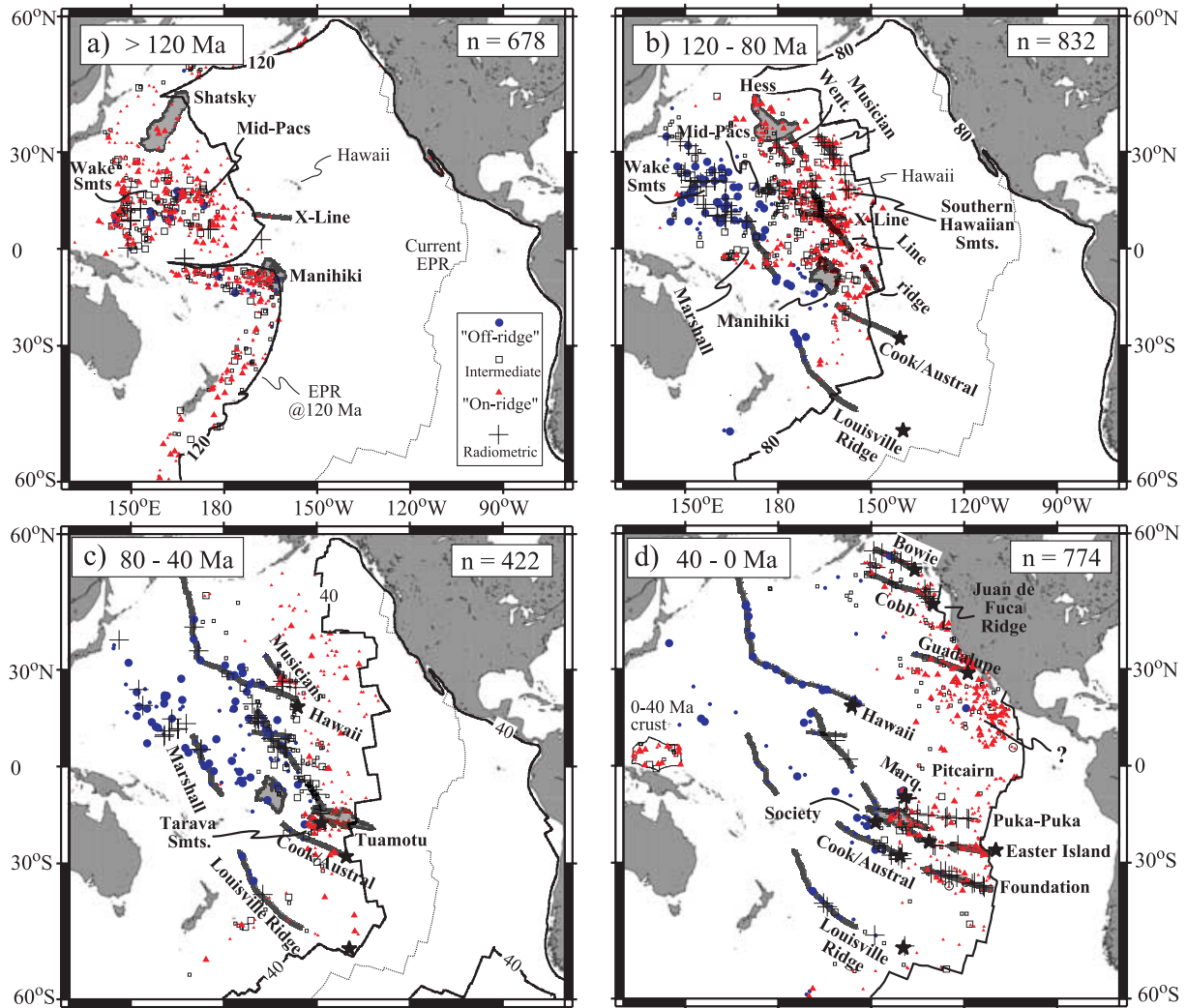


Figure 4. Pacific seamount volcanism in four time periods. ‘On-ridge’, $\Delta t < 20$ Ma, red \blacktriangle . ‘Off-ridge’, $\Delta t > 45$ Ma, blue \bullet . Squares are intermediate Δt . Smaller symbols have basal radius < 20 km. Open circles in d) have $t_{\text{volc}} < 0$ Ma. Where t_{sf} (Müller & Roest 1997) is undated or > 175 Ma, 175 Ma is assumed. Note Cretaceous ‘quiet zone’ (poor dating) is $\sim 120.4\text{--}83.5$ Ma (Gradstein *et al.* 2005). Present day ‘hotspots’ (stars), oceanic plateaus (grey areas), volcanic lineations (grey lines), and spreading ridges (black lines) are for orientation. Crosses are radiometric seamount ages (Koppers *et al.* 2003; Clouard & Bonneville 2005). Line, Line Islands; Marq., Marquesas; Went., Wentworth seamounts; X-Lines, Cross Lines; X, Liliuokalani Ridge (Pringle & Dalrymple 1993). The data plotted is supplied as supplementary material.

trends that consider errors in 1 variable (thin lines). Local studies to determine the ages of seamount chains also suggest that the correlation is real and correct (see Section 3.1).

2.5 Estimating seamount ages

The linear trend fitted to the $GTR_{\text{rel}} - \sqrt{\Delta t}$ data where radiometric ages exist (61 data) establishes a relationship of $GTR_{\text{rel}} = 0.09825\sqrt{\Delta t} + 0.20251$, that is, a relationship between lithospheric strength and seamount age, presuming t_{sf} is known: $t_{\text{volc}} = t_{\text{sf}} - \Delta t$. The trend, shown as the solid thick line on Fig. 3, assumes error in both variables (Marks & Sandwell 1991). It is this trend that is used to estimate an age for each of the 2706 Pacific seamounts shown in Fig. 4. Large seamounts (basal radius > 20 km) have an almost identical trend of $GTR_{\text{rel}} = 0.1036\sqrt{\Delta t} + 0.1486$, shown as the thick dashed line on Fig. 3.

These calibrations of GTR_{rel} against $\sqrt{\Delta t}$ use a subset of the 2706 geophysical strength estimates. As such the 61 strength estimates

used in the calibration benefit from containing exactly the same systematic biases in the flexural model (e.g. assumed load density (ρ_{load}), Poisson’s ratio (ν), or Young’s modulus (E), see Appendix B) as the rest of the 2706 geophysical strength estimates. Thus, systematic biases expected to have little effect on the ‘flexural’ age estimates. For instance, due to some systematic bias GTR_{rel} values could be twice those produced using a model that truly matched reality. The calibration line would then have a gradient twice as steep, but also the 2706 GTR_{rel} values would be twice what they should. A comparison of these GTR_{rel} values to this steepened calibration line in order to deduce flexural ages would thus be unaffected by the systematic bias.

Only one trend is used to describe the calibration data set, on Fig. 3, as there is insufficient evidence to justify a distinct difference between the North Pacific and South Pacific or weak lithosphere in the Superswell region. Perhaps this study’s resolution is insufficient. Alternatively, the ‘abnormal’ seamount chains in French Polynesia (Cook-Austral and Pitcairn) have multiple volcanic episodes

(McNutt 1998) and the GTR method considering only values over the summit may be less affected by this overprinting.

In Fig. 3, 1σ about the mean GTR_{rel} is, on average, 0.130. This translates into $\pm 1.32\sqrt{\Delta t}$ or ~ 1 –11 Ma for a young (4 Ma) seamount and 114–178 Ma for an old (144 Ma) seamount. So uncertainties for individual seamounts are substantial (up to 10s of Ma) but map view plots (Fig. 4) demonstrate patterns for groups of seamounts to be reliable, a validation that is argued for in Section 3.1.

Before this, a justification of complexities in the method for estimating strength, an assessment of the causes of the scatter in the calibration plot, and further computational details are given in the following section.

2.6 Discussion of preferred method and further computational details

The method in Section 2.3 contains some complexities, which are most easily justified by considering methods without them.

The most simplistic way to estimate an observed GTR would be to extract G from the field of Smith & Sandwell (1997), and pick depth from the GEBCO grid (IOC 2003). Seamount height (T) is then depth minus the increase of depth with age of Parsons & Sclater (1977). At the 230 isotopically dated sites in Fig. 1, this gives an r^2 of 0.0023 between GTR and $\sqrt{\Delta t}$.

Following the procedure in this paper up to the end of Section 2.2, more carefully made GTR observations allow an r^2 of 0.1185 between GTR and $\sqrt{\Delta t}$. Like Section 2.3, the correlation and those that follow are calculated at the 61 locations where ‘good quality’ radiometric dates exist. Somewhat arbitrarily excluding 6 outlying GTRs > 100 mGal km $^{-1}$, r^2 is 0.2871. For the large seamounts remaining (basal radius > 20 km), r^2 is 0.4381.

Calculating relative GTR using eq. (1) gives an r^2 of 0.0061 between GTR_{rel} and $\sqrt{\Delta t}$, but this rises to 0.3106 when 5 outlying GTR_{rel} values of > 3 are excluded. For large seamounts remaining after the exculsion r^2 is 0.415. In this case, the exclusion of outliers relates to a theoretically possible range, and as such is less arbitrary, but is still not ideal.

Calculating relative GTR using eq. (2) r^2 between GTR_{rel} and $\sqrt{\Delta t}$ is 0.3800, 0.4489 for large seamounts, and no exclusions are necessary. This simplicity causes this method to be preferred.

A final point regarding the computation of lithospheric strength is that all the computations above are conducted using only a first-order solution to Parker’s equation (Parker 1972) to calculate the gravity anomaly. In theory, higher orders (up to fourth) are important above seamounts (e.g. Watts & Ribe 1984; Lyons *et al.* 2000), however given the spacing of satellite altimeter profiles (every ~ 10 km) these may not be present in the data of used here (anomalies by Wessel & Lyons (1997) using data in Smith & Sandwell (1997)). This appears to be borne out by the r^2 of 0.2899 using the fourth-order solution, compared to 0.3800 for the first-order one.

Scatter in the $GTR_{rel} - \sqrt{\Delta t}$ data on Fig. 3 may, despite the efforts above, still be due to measurement in topography, gravity, or radiometric age. Also, one must also be aware that lithospheric strength relates to emplacement of the bulk of an edifice, whilst radiometric ages come from a sample of the latest activity coating the outside of the volcano. Alternatively, especially for seamounts < 20 km across, uncertainties in GTR_{obs} from a couple of sources are of the same order as the theoretical range ($GTR_{max} - GTR_{min}$). These uncertainties are from ± 100 kg m $^{-3}$ variation in load density, and assumed ‘dimensionality’ of the load (i.e. 2-D ridge versus 3-D cone) (Ribe 1982; Cazenave & Dominh 1984; Watts *et al.* 1988;

Lyons *et al.* 2000). However ages estimated from GTR_{rel} in Section 2.5 along the Louisville Ridge, which is quasi-continuous to the north and isolated edifices to the south, follow the NW-to-SE progression with time indicated by radiometric dating. This suggests that dimensionality variations do not corrupt this analysis. Crustal thickness (± 1 km), and crustal, infill and mantle density variations (± 100 kg m $^{-3}$) have only a relatively minor effect.

The effect of varied deviations from the simple thin elastic plate model (Fig. 2) probably required to accurately model reality may also cause scatter, but are difficult to assess. For example, Watts & Ribe (1984) document the effect of variable infill density (allows bluges to be modelled accurately), laterally variable T_e and a plate fractured under the load. Inelastic yielding, stress relaxation, a thick plate and underplating may also be required and are discussed in Watts (2001). It is also noted that the interpretation of effective plate thickness T_e with respect to crustal thickness and indicators of material properties causing the strength (seismogenic thickness, mantle xenoliths, tomography) are currently debated (e.g. Maggi *et al.* 2000; Watts & Burov 2003; McKenzie *et al.* 2005). However, since we do not interpret further than requiring strength estimates to correlate with radiometric ages ($\sqrt{\Delta t}$), the simple model is a perfectly valid one to date seamounts with.

3 RESULTS

After quality control 121 882 seamounts (3874 > 1.5 km tall) are extracted from echo-sounder data, of which 2706 ($\sim 1/3$) match one of 7968 gravity anomalies (Wessel & Lyons 1997). For these, a measure of lithospheric strength has been calculated, and presuming the seamounts to be volcanoes they are associated with a Δt (i.e. tectonic setting) based on a self-consistent calibration using a subset of locations where radiometric dates exist.

Fig. 4 shows the distribution of on-ridge (\blacktriangle) and off-ridge (\bullet) Pacific seamount volcanism ($n_{tot} = 2706$) during four time intervals, which are plotted on current-day maps. From flexurally estimated values of Δt , seamount age, t_{volc} , is calculated from seafloor ages (Müller & Roest 1997), t_{sf} , using $t_{volc} = t_{sf} - \Delta t$. The division between eruption into ‘on-ridge’, $\Delta t < 20$ Ma, and ‘off-ridge’, $\Delta t > 45$ Ma, tectonic settings, that is, onto young and old lithosphere, is chosen to emphasise patterns documented from localised studies, but is not dissimilar to the speculative values of 2–8 Ma and > 35 Ma used by Watts *et al.* (1980). Given doubt that may be expressed about the strength of correlation in Fig. 3, a validation of the geophysically estimated volcanic ages against other age estimates is important.

3.1 Validation

A basic level validation is obtained from the general distribution of the estimated ages in Fig. 4. First, almost all data plot west of the spreading centre (i.e. on crust that has been created). This is expected of a ‘correct’ $GTR_{rel} - \sqrt{\Delta t}$ relationship, but in no way required by the conversion of strength estimates into ages. Secondly, basin-wide west-to-east, off-ridge to on-ridge progressions in the time intervals are consistent with older seafloor in the western Pacific. Finally, the geophysically predicted ages coincide spatially with radiometric estimates (+), which supports the predictions as the calibration does not require seamounts to plot in the *right place* at the right time. Note that spatial coincidence does not exist for arbitrary relationships, such as $\Delta t = 20$ Ma. Any *en masse* determination of age or tectonic setting should pass tests such as these.

More specifically, geophysical estimates of t_{volc} are in accord with literature determinations of tectonic setting (either by T_e , radiometric dates, isotopes, magnetics, geochemistry, subsidence analysis). These agreements are summarised below; Hillier (2005) gives more detail, and Clouard & Bonneville (2005) collate radiometric ages.

(i) Oceanic plateaus (on-ridge): Shatsky Rise, 145–135 Ma (Den *et al.* 1969; Marks & Sandwell 1991; Sager & Han 1993; Nakanishi *et al.* 1999; Sager *et al.* 1999; Verzhbitskii & Merklin 2000); Hess Rise, ~100 Ma (Windom *et al.* 1981; Vallier *et al.* 1983; Marks & Sandwell 1991); Manihiki Plateau, 124–118 Ma (Hussong *et al.* 1979; Mahoney & Spencer 1991; Tarduno *et al.* 1991; Coffin & Eldholm 1993; Ito & Clift 1998), with late-stage reactivation at ~70 Ma (Bercovici & Mahoney 1994; Ito & Clift 1998); Tumaotu Plateau, ~40 Ma (Talandier & Okal 1987; Ito *et al.* 1995; McNutt 1998; Patriat *et al.* 2002).

(ii) Volcanic groups forming at divergent plate boundaries (on-ridge): Musicians, ~95–75 Ma (Schwank & Lazarewicz 1982; Dixon *et al.* 1983; Freedman & Parsons 1986; Kopp *et al.* 2003) and the geophysical ages record a previously observed (Schwank & Lazarewicz 1982) north to south volcanic progression through time; Cobb hotspot trace, 20–0 Ma (e.g. Desonie & Duncan 1990); Foundation seamounts 20–0 Ma (Mammerickx 1992; Devey *et al.* 1997; O'Connor *et al.* 1998; Maia *et al.* 2001; Maia & Hamed 2002); Guadalupe chain (e.g. Koppers *et al.* 2001). Puka-Puka Ridge was also formed on young lithosphere (Sandwell *et al.* 1995).

(iii) Intraplate volcanic groups (off-ridge): Hawaiian chain, 0–65 Ma (Wilson 1963a,b; Moore & Clague 1992); Louisville Ridge, 0–80 Ma (Cazenave & Dominh 1984; Cheng *et al.* 1987; Hawkins *et al.* 1987; Watts *et al.* 1988; Lyons *et al.* 2000); Marquesas, 0–40 Ma (Filmer *et al.* 1993; Caress *et al.* 1995; McNutt 1998); Society 0–40 Ma (Filmer *et al.* 1993; Clouard & Bonneville 2001). Marshall-Gilbert seamounts, few radiometric dates ~80 Ma (Davis *et al.* 1989), 60–70 Ma (Koppers & Staudigel 2005), ~50 Ma (Kulp 1963) also bio-stratigraphic dates (Lincon *et al.* 1993).

(iv) Volcanic groups or chains with multiple volcanic episodes: Line Islands, Cretaceous and Mid-Eocene (~50–38 Ma) (radiometric and paleomagnetic data) (Haggerty *et al.* 1982; Schlanger *et al.* 1984; Sager & Keating 1984; Davis *et al.* 2002); Marcus-Wake seamounts, 100–85 Ma (McNutt *et al.* 1990), possibly up to 130 Ma (Heezen *et al.* 1973). Kodiak-Bowie (a.k.a Pratt-Weckler) chain; 0–20 Ma (K-Ar dating, geochemistry and subsidence analyses) (Turner *et al.* 1980; Lambeck *et al.* 1984; Cousens *et al.* 1985; Harris & Chapman 1989, 1991). Cook-Austral alignment; between 60 and 0 Ma (Woodhead 1996; Chauvel *et al.* 1997; McNutt *et al.* 1997; Dickinson 1998).

This good agreement between flexurally estimated volcanic ages and dating from other sources gives strong support to the predictions. It is probably worth noting that plotting flexural ages in four time periods is a tougher test of these predictions than using a single plot. The Hawaiian-Emperor chain, 0–65 Ma (e.g. Wilson 1963a,b; Moore & Clague 1992), for example, are off-ridge along their length (except the northern tip) as the results of Watts *et al.* (1980), and show as this if Figs 4(a)–(d) are condensed onto a single plot (Data supplied in supplementary material). However, some Hawaiian volcanoes plot in Fig. 4(c) and some Emperor Chain seamounts in Fig. 4(d). It is uncertain what causes this but the Hawaiian Swell, flexural bulge from trenches to the north, or the Emperor chain passing between the Hess and Shatsky Rises may be involved. As a counter-case, volcanism along the Louisville chain progresses as expected.

3.2 New observations and implications

Radiometric dates are few and dominantly from recent hotspot volcanism, so a key advantage of ‘flexural ages’ is that they are more likely to constitute a representative distribution of seamount volcanism. It is, therefore, possible to better comment upon the distribution of Pacific volcanism across space and time.

First-order patterns presented in Fig. 4 are a strip of on-ridge volcanism from Easter Island through the Tuamotu Plateau to the Line Islands, and off-ridge volcanism most dominant in the NW Pacific.

On-ridge volcanism tends to occur in spatially diffuse groups such as by the Wake seamounts and Mid-Pacific Mountains in Fig. 4(a) and south of Guadalupe on Fig. 4(d), but also shows many elongated trends (e.g. Wentworth seamounts, Foundation seamounts) although these are not as strictly linear as the off-ridge trends. Off-ridge volcanism is dominantly in lineations (e.g. Hawaii-Emperor Chain, Louisville Ridge), but also occurs in a diffuse grouping upon the oldest seafloor in the NW Pacific. This demonstrates that a division between diffuse on-ridge volcanism and lineated off-ridge volcanism as suggested by Watts *et al.* (1980) is not necessarily adhered to.

From Fig. 4 it can be observed that multiple ages of volcanism commonly appear to occupy the same area of seafloor, for example, around the Line Islands. Alternatively phrased, geologically defined regions may mix of both on-ridge and off-ridge tectonic settings. This implies prolonged periods of activity, or quiescence then reactivation. Minimal off-ridge activity in places such as Hess Rise and the Musicians imply that the mixture is not just an artefact due to scatter caused by the method. Where two or three generations of volcanism occur in close proximity, T_e estimation is difficult (McNutt 1998), but just using GTR values over seamounts’ summits could act to reduce the influence of neighbouring edifices.

A region where prolonged activity (~160–75 Ma) seems to have occurred is in the old NW Pacific around the Wake seamounts. This area is most clearly shown by the cluster of off-ridge activity in Fig. 4(b). Similar is true, though less obviously, for the Mid-Pacific Mountains. Interestingly, volcanism initiated near a spreading centre, but continued in the same region well after the ridge is distant, implies a lithospheric (as opposed to asthenospheric) component to the mechanism that controls the location of volcanism.

French Polynesia also exhibits enduring volcanic activity, but along lineaments. On-ridge activity starts at the NW end of the Cook-Austral alignment in (b), moves to near the present day Pitcairn hot spot in (c), and continues ESE along the Foundation chain in (d). Later, off-ridge volcanism starts in (c), again at the NW end of the alignment, and occurs along the alignment in (d) presumably related to the current day hot spot. A somewhat similar relationship (later hot spot on pre-existing volcanic chain) appears to exist between the Easter Island chain and Pitcairn hot spot. One explanation for these patterns could be that the first on-ridge episode facilitated or influenced the later off-ridge one. Perhaps fresh volcanism occurs as on-ridge chains move west on the Pacific plate and encounter anomalous asthenosphere thought to exist there (see SOPITA, superplume (Larson 1991), and Darwin Rise (Menard 1964)). A possible mechanism for the facilitation, proposed at Mid-Ocean Ridges (Niu & Batiza 1993; Aharanov *et al.* 1995; Kelemen *et al.* 1997), is that melt–matrix interaction creates low-permeability dunnite conduits. Alternatively, the stress field imposed by existing edifices, through cracking, could govern where volcanoes erupt (e.g. Ten Brink 1991).

More specific original observations from Fig. 4 include the following:

(i) In (a) and (b), the Cross Lines are poorly dated, but flexural ages indicate that they formed in the Cretaceous near, and at a high angle to, a spreading ridge. The Easter Island and Foundation chains may be modern analogues of this near-ridge formation. Flexural ages also indicate less prevalent later off-ridge activity in the Cross Lines.

(ii) In (b), flexural ages supplement sparse observations of the Wentworth seamounts (Watts *et al.* 1980; Pringle & Dalrymple 1993) and provide the first age indication for the 'Liliuokalani Ridge' (Pringle & Dalrymple 1993) immediately to the east. Both appear on-ridge, so are probably related to the formation of the Hess Rise.

(iii) In (b), the Musicians and the Southern Hawaiian seamounts (a.k.a Geologist Seamounts) (Sager & Pringle 1987) start to form contemporaneously near the ridge crest from ~100 Ma, the gap between the two probably explained by ridge geometry still visible in the 80 Ma isochron. Volcanism along this 'soft' Musicians-Geologists alignment, then continues as the ridge moves away. Tentatively, note that the recent trace of the Hawaiian hotspot (last several Ma) appears to divert to the south along this alignment, perhaps explained if lithosphere previously subject to volcanism is more easily permeable to subsequent melt. In caution, note that seafloor here has few magnetic reversals (Cretaceous quiet zone), which contributes to uncertainties (e.g. Kopp *et al.* 2003).

(iv) In (c) volcanism 200–300 km SW of the current Society hot spot is on-ridge. The volcanism is called the Tavara seamounts (formerly the Savannah seamounts (Bonneville *et al.* 1997; Sichoix *et al.* 1998; Hillier & Watts 2004)), and the Va'a Tau Piti Ridges. Clouard & Bonneville (2003) find 'on-ridge' T_e values of 8 and 3 km, respectively. If 2 K/Ar dredge haul ages of 43 and 36 Ma are trusted (see Baksi 2005; Clouard & Bonneville 2005), however, they indicate an off-ridge tectonic setting. A scenario where early large-volume volcanism is covered with a later veneer of off-ridge volcanism would reconcile these observations. The volcanism SW of Society shares several features with the Musicians; on-ridge tectonic setting, proximity to a transform fault, predicted morphology (Smith & Sandwell 1997), and very low T_e ridges approximately parallel to fracture zones (i.e. were approximately perpendicular to the spreading ridge). So, mechanisms of origins may be similar.

(v) In (d), on-ridge activity clustered south of Guadalupe coincides with a broad region of shallow seafloor and slow tomographic velocities in the depth range 0–125 km (Hillier & Watts 2004). If the observations have a common origin, they may indicate enhanced mantle melting leading to regionally thick crust, or alternatively imply a thermally thin lithosphere. Whatever mechanism is selected, however, this is a good indication that the oceanic lithosphere does not form homogeneously along a ridge or through time. Thus, any planform of large-scale bathymetric anomalies may substantially relate to processes creating the plate at the ridge and not to processes such as mantle convection.

4 DISCUSSION

It has become something of an orthodoxy to associate weak lithosphere, measured by low T_e values, with an 'on-ridge' tectonic setting; namely volcanic loads applied to young seafloor (low Δt) in the proximity of an oceanic spreading centre. The primary evidence for this relationship between T_e and Δt comes from compilations such as that of Watts (2001) where Δt is independently estimated, generally using radiometric dates. High T_e is similarly linked to 'off-ridge'. So, in flexural studies the terms 'on-ridge' and 'off-ridge' implicitly assign formation dates to oceanic features, albeit approx-

imate ones. The steps made in creating this link are; determining strength, calibrating strengths against independently obtained age data, and then associating strengths with ages.

This work automates the above steps and self-consistently combines them into a single paper. This harmonises the computational method and physical properties used, but automation probably introduces some scatter. However, a link between lithospheric strength and Δt , and thus volcano age, has been established. Here, instead of just quoting tectonic setting, strengths are converted into ages. With estimated uncertainties in the order of 10 Ma (see Section 2.5) this may be pushing the data, but conversion into ages is favoured as it offers a direct, numerical, and perhaps stark, comparison to chronological constraints from other sources. The flexural ages estimated here appear to withstand such a comparison in the validation, and the data is given as a supplementary table for future comparisons.

Converting to ages also permits an examination of the rate of volcanic activity through time and, unlike previous studies, a division into tectonic settings is possible giving insights into magmatic processes.

4.1 Rate through time

Fig. 5(a) is a histogram of how the volume of seamount volcanism distributes itself across oceanic seafloor of different ages. There are two main peaks of activity centred upon seafloor of 160–150 and 120–110 Ma, respectively spanning 170–140 Ma and 130–100 Ma (convex curves). Most obviously in these peaks, on-ridge through to off-ridge volcanism occurs on the same age of seafloor (bold vertical arrows). This indicates volcanism over a long duration through the same lithosphere. There is also an increase in volume from 60 Ma to 0 Ma seafloor.

Fig. 5(b) is a histogram of the volume of seamount volcanism through time. The two peaks of activity above are detectable (convex curves and arrows), but overall pattern now has a dominant peak between 80 and 120 Ma. Volcanism before this is quite high, afterwards dips around 60 Ma, and has a broad subsidiary peak centred around 30 Ma. Volcanism is dominantly (>1/2) on-ridge. Off-ridge volcanism is a quasi-constant between 30 and 120 Ma, but most voluminous between 30 and 50 Ma, is reduced below 30 Ma, and by definition not present before 130 Ma.

The most comparable previous curves to Figs 5(a) and 5(b) are those of Smith (1990) and of Wessel & Lyons (1997), shown on Fig. 5(c). Smith's curve of volcanism upon seafloor of a given age and Fig. 5(a) both have the peak at ~120 Ma, but Smith does not find the one at 160–150 Ma, or the increase from 60 Ma. The increase is much reduced when the normalized for seafloor area (km^3/km^2), so is partly due to the increasing area of young seafloor, but relatively easy altimetric detection of seamounts on young shallow seafloor is probably also a factor.

If total volcanism through time is considered Fig. 5(b) looks rather similar to that deduced for his 'pseudo-ages' by Wessel & Lyons (1997), despite the cautions about this data stated in the introduction. The broad eruptive peak spans 120–80 Ma. It starts with the Ontong-Java Plateau (Eldholm & Coffin 2000) and coincides with a period of high crustal production at mid-ocean ridges. Large Igneous Province (LIP) volcanism (Fig. 4d) (Eldholm & Coffin 2000) and seamount volcanism do not seem to affect long-term strontium isotopes, oxygen isotopes or sea-level (Figs 5e–g), which it is reasonable to assume are controlled by mid-ocean ridge spreading (Jones & Jenkyns 2001). It appears however that seafloor spreading, perhaps assisted by seamount volcanism, sets the conditions between 120

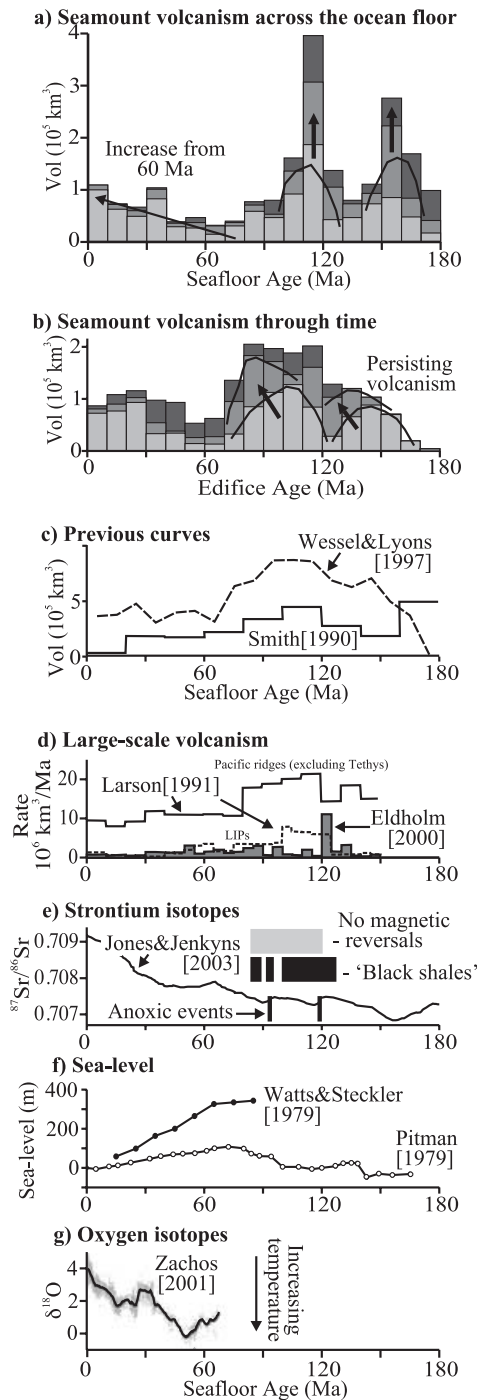


Figure 5. Volcanism through time. (a) Histogram of seamount volume as a function of underlying seafloor age. Light ($n = 1388$), medium ($n = 613$) and dark ($n = 323$) shades indicate on-ridge, intermediate and off-ridge settings, respectively. Total number, 2324, is less than 2706 (Fig. 4) as the aim here is not to best represent the spatial distribution, rather that through time, and so only seamounts with $t_{sf} < 175$ Ma are used. (b) Histogram of volcanic volume erupted through time. On-ridge ($n = 1285$), flank ($n = 536$), and off-ridge ($n = 272$) shaded as before. Total number displayed, 2093, is less than 2324 as t_{volc} for some edifices is < 0 Ma. Note: For total volcanic volume, add volume of compensating material, V_c , to edifice volume V_e ; $V_c = (\rho_{load} - \rho_{water}) / (\rho_{mantle} - \rho_{infill})$ whatever T_e is. (c)–(g) are literature curves for comparison (see text). Period of no magnetic reversals dated by Gradstein *et al.* (2005). Note that Eldholm & Coffin's (2000) compilation contains additional age constraints to Larson (1991) and unlike Larson they do not double volumes to allow for hypothesised subducted 'twins'.

and 80 Ma for the environmentally stressful conditions to create 'black shales' (Jenkyns 1980), and allow LIP volcanism at ~ 120 and ~ 90 Ma to cause ocean-wide anoxic events as well as short term variations in the strontium isotope curve (Jones & Jenkyns 2001; Jenkyns 2003). The volcanism at 120 Ma also appears to have caused extinction and a marine biological crisis (Coffin & Eldholm 1994; Erba 1994; Sinton & Duncan 1997; Kerr 1998; Larson & Erba 1999).

Whilst seamount volcanism is much less voluminous than LIP volcanism and crustal production at the spreading ridges, the geometry of seamounts may amplify their effects. Being close to the ocean's surface, rising plumes can more easily impact upon shallow waters that are an important in some models (e.g. Larson & Erba 1999). Similarly, recent numerical modelling of chemical transport also indicates that seamount formation may impact disproportionately and 'contribute to globally significant hydrothermal fluxes' (Harris *et al.* 2004).

Instead of the total volcanic volumes, it is the division into tectonic settings that provides evidence regarding the mechanism behind seamount volcanism. Both Figs 5(a) and 5(b) show 2 peaks of activity (convex curves and arrows) indicate volcanism over a long duration through the same lithosphere, in these cases around the Wake Seamounts and Mid-Pacific Mountains (1st peak) and the Line Islands (2nd peak). This reiterates the observations of persisting volcanism through lithosphere as it moves a considerable distance over the asthenosphere in Fig. 4, which again imply a strong lithospheric component to the mechanism controlling the location of volcanism. As for the chains in French Polynesia, a possible mechanism for this proposed at Mid-Ocean Ridges (Niu & Batiza 1993; Aharanov *et al.* 1995; Kelemen *et al.* 1997) is that melt–matrix interaction creates low-permeability dunnite conduits. Alternatively, the stress field imposed by existing edifices, through cracking, could govern where volcanoes erupt (e.g. Ten Brink 1991).

5 CONCLUSIONS

It is demonstrated that automated, self-consistent, basin-wide estimation of lithospheric strength (GTR_{rel}) at the time of volcanic loading (Δt) is possible in the Pacific using the ratio of gravity to topography above the summits of volcanoes. These strength estimates are shown to correlate with directly sampled, radiometric, ages. At the accuracy of this study, only one strength– $\sqrt{\Delta t}$ relationship is required for the Pacific; $GTR_{rel} = 0.09825\sqrt{\Delta t} + 0.20251$. Using this, it is for the first time possible to assign eruption ages *en masse*, specifically to 2706 volcanoes. Validation proves these 'flexural ages' are at least accurate enough to determine the tectonic setting of volcanic emplacement (i.e. on-ridge and off-ridge), make maps of seamount volcanism through time, and construct histograms of activity.

The flexural ages show that: A division between diffuse on-ridge volcanism and lineated off-ridge volcanism as suggested by Watts *et al.* (1980) is not necessarily adhered to; Variation in the spatial density of on-ridge volcanoes on 0–80 Ma seafloor supports the idea that oceanic lithosphere does not form homogeneously along a ridge or through time; The Cross Lines are on-ridge and ~ 120 – 110 Ma; The Wentworth Seamounts and Liliuokalani Ridge are probably connected to the formation of the Hess Rise.

Perhaps the most significant observation, however, is of widespread recurrences of volcanism proximal to older features, namely a mix of tectonic setting within geological regions. Prominently, this occurs in regions such as the oldest seafloor in the NW

Pacific, and within volcanic chains such as Cook-Austral and Pitcairn in French Polynesia. The former is seemingly persisting volcanism through the same lithosphere even as it moves substantially over the asthenosphere, and the later reactivation of chains as they encounter more fertile asthenosphere. What both appear to signify, however, is that the lithosphere exerts a significant element of control upon the location of volcanism, and that magmatic throughput leaves the lithosphere more susceptible to the passage of future melts.

ACKNOWLEDGMENTS

I thank Tony Watts, Katie Johnston and members of the Marine Lab. Many figures were produced using GMT software. JH supported by NERC. I also thank A. Bonneville, T. Minshull and an anonymous reviewer for their constructive comments.

REFERENCES

- Aharanov, E., Whitehead, J.A., Kelemen, P.B. & Spieglerman, M., 1995. Channelling instability of upwelling melt in the mantle, *J. geophys. Res.*, **100**(B10), 20 433–20 450.
- Baksi, A.K., 2005. Evaluation of radiometric ages pertaining to rocks hypothesized to have been derived by hotspot activity, in and around the Atlantic, Indian, and Pacific oceans, in *Plates, Plumes and Paradigms*, pp. 55–70, eds Foulger, G.R., Natland, J.H., Presnall, D.C. & Anderson, D.L., Geological Society of America Special Paper 388.
- Batiza, R., 1982. Abundances, distribution and sizes of volcanoes in the Pacific Ocean and implications for the origin of non-hotspot volcanoes, *Earth planet. Sci. Lett.*, **60**, 195–206.
- Bercovici, D. & Mahoney, J., 1994. Double flood basalts and plume head separation at the 660-kilometre discontinuity, *Science*, **266**, 1367–1369.
- Bonneville, A., Clouard, V., Beuzart, P., Klaucke, I., Suave, R.L., Loubrieu, B., Saget, P. & Thomas, Y., 1997. Possible control of Society Islands volcanism by a preexisting volcanic chain, *EOS, Trans. Am. geophys. Un.*, **78**(46), 725, Fall Meet. Suppl., Abstract T52B-02.
- Bridges, N.T., 1997. Characteristics of seamounts near Hawaii as viewed by GLORIA, *Mar. Geol.*, **138**, 273–301.
- Calmant, S., Francheteau, J. & Cazenave, A., 1990. Elastic layer thickening with age of the oceanic lithosphere—a tool for prediction of the age of volcanoes or oceanic-crust, *Geophys. J. Int.*, **100**(1), 59–67.
- Caress, D.W., McNutt, M.K., Detrick, R.S. & Mutter, J.C., 1995. Seismic imaging of hot spot-related underplating beneath the Marquesas Islands, *Nature*, **373**, 600–603.
- Carlson, R.L. & Herrick, C.N., 1990. Densities and porosities in the oceanic crust and their variations with depth and age, *J. geophys. Res.*, **95**(B6), 9153–9170.
- Carter, D.J.T., 1980. *Echo-Sounding Correction Tables*, 3rd edn, Hydrographic Department, Ministry of Defence, Taunton, Somerset, UK.
- Cazenave, A. & Dominh, K., 1984. Geoid heights over the Louisville Ridge (South Pacific), *J. geophys. Res.*, **89**(B13), 11 171–11 179.
- Chauvel, C., McDonough, W., Guille, G., Maury, R. & Duncan, R., 1997. Contrasting old and young volcanism in Rurutu Island, Austral chain, *Chem. Geol.*, **139**, 125–143.
- Cheng, Q., Park, K.H., McDougall, J.D., Zindler, A., Langmuir, G.W., Staudigel, H., Hawkins, J. & Lonsdale, P., 1987. Isotopic evidence for a hot spot origin of the Louisville seamount chain, in *Seamounts, Islands and Atolls Geophys. Mono.* 43, pp. 283–293, eds Keating, B.H., Fryer, P., Batiza, R. & Boehlert, G.W., American Geophysical Union, Washington DC.
- Clouard, V. & Bonneville, A., 2001. How many Pacific hot-spots are fed by deep-mantle plumes? *Geology*, **29**, 695–698.
- Clouard, V. & Bonneville, A., 2003. The tavana seamounts: A newly characterized hotspot chain on the south Pacific superswell, *Earth planet. Sci. Lett.*, **207**, 117–130.
- Clouard, V. & Bonneville, A., 2005. Ages of seamounts, islands, and plateaus on the Pacific plate, in *Plates, Plumes and Paradigms*, pp. 71–90, eds Foulger, G.R., Natland, J.H., Presnall, D.C. & Anderson, D.L., Geological Society of America Special Paper 388.
- Coffin, M. & Eldholm, O., 1993. Scratching the surface: Estimating dimensions of large igneous provinces, *Geology*, **21**, 515–517.
- Coffin, M. & Eldholm, O., 1994. Large igneous provinces—crustal structure, dimensions, and external consequences, *Rev. Geophys.*, **32**, 1–36.
- Cousens, B.L., Chase, R.L. & Schilling, J.G., 1985. Geochemistry and origin of volcanic rocks from Tuzo-Wilson and Bowie seamounts, *Can. J. Earth Sci.*, **22**(11), 1609–1617.
- Craig, C.H. & Sandwell, D.T., 1988. Global distribution of seamounts for Seasat profiles, *J. geophys. Res.*, **93**(B9), 10 408–10 420.
- Dantzig, G.B., 1963. *Linear Programming and Extensions*, Princeton University Press, Princeton, New Jersey.
- Davis, A.S., Pringle, M.S., Pickthorn, L.B.G., Clague, D.A. & Shawab, W.C., 1989. Petrology and age of alkalic lava from the Ratak chain of the Marshall Islands, *J. geophys. Res.*, **94**(B5), 5757–5774.
- Davis, A.S., Gray, L.B., Clague, D.A. & Hein, J.R., 2002. The Line Islands revisited: New Ar-40/Ar-39 geochronologic evidence for episodes of volcanism due to lithospheric extension, *Geochem. Geophys. Geosys.*, **3**, art. no. 1018, doi 10.1029/2001GC000190.
- Den, N. *et al.*, 1969. Seismic-refraction measurements in the northwest Pacific Basin, *J. geophys. Res.*, **74**(6), 1421–1435.
- Desonie, D.L. & Duncan, R.A., 1990. The Cobb-Eickelberg seamount chain: Hot spot volcanism with mid-ocean ridge basalt affinity, *J. geophys. Res.*, **95**(B8), 12 697–12 711.
- Devey, C.W. *et al.*, 1997. The Foundation seamount chain: a first survey and sampling, *Mar. Geol.*, **137**(3–4), 191–200.
- Dickinson, W.R., 1998. Geomorphology and geodynamics of the Cook Austral island seamount chain in the South Pacific ocean: implications for hot spots and plumes, *Int. Geol. Rev.*, **40**(12), 1039–1075.
- Dixon, T.H., Naraghi, M., McNutt, M.K. & Smith, S.M., 1983. Bathymetric prediction for seasat altimeter data, *J. geophys. Res.*, **88**(NC3), 1563–1571.
- Eldholm, O. & Coffin, M., 2000. *Large Igneous Provinces and Plate Tectonics*, Vol. 121, pp. 309–326, American Geophysical Union.
- Epp, D., 1984. Implications of volcano and swell heights for thinning of the lithosphere by hot spots, *J. geophys. Res.*, **89**(B12), 9991–9996.
- Erba, E., 1994. Nannofossils and superplumes - The early Aptian nannoconid crisis, *Paleoceanography*, **9**(3), 483–501.
- Filmer, P.E., McNutt, M.K. & Wolfe, C.J., 1993. Elastic thickness of the lithosphere in the Marquesas and Society islands, *J. geophys. Res.*, **98**, 19 565–19 577.
- Freedman, A.P. & Parsons, B., 1986. Seasat-derived gravity over the Musicians seamounts, *J. geophys. Res.*, **91**(B8), 8325–8340.
- Gradstein, F.M., Ogg, J.G., Smith, A.G., Bleeker, W. & Lourens, L.J., 2005. A new geologic time scale, with special reference to Precambrian and Neogene, *Episodes*, **27**(2), 83–100.
- Gunn, R., 1943. A quantitative study of isobaric equilibrium and gravity anomalies in the Hawaiian islands, *J. Franklin Institute*, **236**, 373–390.
- Haggerty, J.A., Schlanger, S.O. & Silva, I.P., 1982. Late Cretaceous and Eocene volcanism in the southern Line Islands and implications for hot spot theory, *Geology*, **10**, 433–437.
- Hammer, P.T.C., Dorman, L.M., Hildebrand, J.A. & Cornuelle, B.D., 1994. Jasper seamount structure—Sea-floor seismic-refraction tomography, *J. geophys. Res.*, **99**(B4), 6731–6752.
- Hammond, S.R., 1997. Offset caldera and crater collapse on Juan de Fuca ridge-flank volcanoes, *Bull. Volcanol.*, **58**, 617–627.
- Harris, R.N. & Chapman, D.S., 1989. The Bowie hot spot, *EOS, Trans. Am. geophys. Un.*, **70**, 1358, Fall Meeting Supplemental.
- Harris, R.N. & Chapman, D.S., 1991. Lithospheric flexure associated with the Queen Charlotte Trough and the southern Kodiak-Bowie seamount chain, northeast Pacific, *EOS, Trans. Am. geophys. Un.*, **72**, 473, Fall Meeting Supplemental.

- Harris, R.N., Fisher, A.T. & Chapman, D.S., 2004. Fluid flow through seamounts and implications for global mass fluxes, *Geology*, **32**(8), 725–728, 10.130/G20387.1.
- Hawkins, J.W., Lonsdale, P. & Batiza, R., 1987. Petrologic evolution of the Louisville seamount chain, in *Seamounts, Islands and Atolls Geophys. Mono.* 43, pp. 235–247, eds Keating, B.H., Fryer, P., Batiza, R. & Boehlert, G.W., American Geophysical Union, Washington DC.
- Heezen, B.C., Matthews, J.L., Catalano, R., Natland, J., Coogan, A., Tharp, M. & Rawson, M., 1973. Western Pacific guyots, *Initial Reports of the Deep Sea Drilling Project*, **20**, 653–700.
- Hillier, J.K., 2005. The Bathymetry of the Pacific Ocean Basin and its Tectonic Implications, *PhD thesis*, University of Oxford, Chapter 4: Pacific Seamount Volcanism in Space and Time.
- Hillier, J.K. & Watts, A.B., 2004. 'Plate-Like' subsidence of the East Pacific rise—South Pacific superswell system, *J. geophys. Res.*, **109**(B10102), doi 10.1029/2004JB003041.
- Hillier, J.K. & Watts, A.B., 2005a. The relationship between depth and age in the North Pacific ocean, *J. geophys. Res.*, **110**(B02405), doi 10.1029/2004JB003406.
- Hillier, J.K. & Watts, A.B., 2005b. Pacific seamount volcanism in space and time, *Geophysical Research Abstracts*, **7**, Abs. no. 01324.
- Hussong, D.M., Wiperman, L.K. & Kroenke, L.W., 1979. The crustal structure of the Ontong Java and Manihiki oceanic plateaus, *J. geophys. Res.*, **84**(B11), 6003–6010.
- Hyndman, R.D., Christensen, H.I. & Drury, M.J., 1979. Seismic velocities, densities, electrical resistivities, porosities and thermal conductivities of core samples from boreholes into the islands of Bermuda and the Azores, in *Deep Drilling Results in the Atlantic Ocean: Ocean Crust*, pp. 94–112, eds Talwani, M., Harrison, C.G. & Hayes, D.E., Maurice Ewing Series 2, AGU.
- IOC, 2003. GEBCO 1-minute grid, <http://www.ngdc.noaa.gov/mgg/gebco/>, GEBCO is associated with British Oceanographic Data Centre (BODC), and operates under the auspices of the International Hydrographic Organisation (IHO) and the United Nations' (UNESCO) Intergovernmental Oceanographic Commission (IOC).
- Ito, G. & Clift, P.D., 1998. Subsidence and growth of Pacific Cretaceous plateaus, *Earth planet. Sci. Lett.*, **161**, 85–100.
- Ito, G., McNutt, M. & Gibson, R.L., 1995. Crustal structure of the Tuamotu Plateau, 15-degrees-S, and implications for its origin, *J. geophys. Res.*, **100**, 8097–8114.
- Jenkyns, H.C., 1980. Cretaceous anoxic events: From continents to oceans, *J. Geol. Soc. Lond.*, **137**, 171–188.
- Jenkyns, H.C., 2003. Evidence for rapid climate change in the Mesozoic-Palaeogene greenhouse world, *Phil. Trans. Roy. Soc. Lond., Ser. A* **361**, 1885–1916.
- Jones, C.E. & Jenkyns, H.C., 2001. Seawater strontium isotopes, ocean anoxic events, and seafloor hydrothermal activity in the Jurassic and Cretaceous, *Am. J. Sci.*, **301**(2), 112–149.
- Jordan, T.H., Menard, H.W. & Smith, D.K., 1983. Density and size distribution of seamounts in the eastern Pacific inferred from wide-beam sounding data, *J. geophys. Res.*, **88**, 10 508–10 518.
- Kelemen, P.B., Hirth, G., Shimizu, N., Spiegelman, M. & Dick, H.J.B., 1997. A review of melt migration processes in adiabatically upwelling mantle beneath oceanic spreading ridges, *Phil. Trans. R. Soc. Lond., Ser. A* **355**, 283–318.
- Kerr, A.C., 1998. Oceanic plateau formation: A cause of mass extinction and black shale deposition around the Cenomanian-Turonian boundary? *J. Geol. Soc. Lond.*, **155**, 619–626.
- Kopp, H., Kopp, C., Morgan, J.P., Flueh, E.R., Weinrebe, W. & Morgan, W.J., 2003. Fossil hot spot-ridge interaction in the Musicians seamount province: Geophysical investigations of hot spot volcanism at volcanic elongated ridges, *J. geophys. Res.*, **108**(B3), art. no. 2160, doi 10.1029/2002JB002015.
- Koppers, A.A.P. & Staudigel, H., 2005. Asynchronous bends in Pacific seamount trails: a case for extensional volcanism? *Science*, **307**(5711), 904–907.
- Koppers, A.A.P., Morgan, J.P., Morgan, J.W. & Staudigel, H., 2001. Testing the fixed hot spot hypothesis using Ar-40/Ar-39 age progressions along seamount trails, *Earth planet. Sci. Lett.*, **185**, 237–252.
- Koppers, A.A.P., Staudigel, H., Pringle, M.S. & Wijbrans, J.R., 2003. Short-lived and discontinuous intraplate volcanism in the South Pacific; hot spots or extensional volcanism, *Geochem. Geophys. Geosys.*, **4**, art. no. 1089.
- Kulp, J.L., 1963. Potassium-argon dating of volcanic rocks, *Bull. Volcanol.*, **26**, 247–258.
- Lambeck, K., Penny, C.L., Nakiboglu, S.M. & Coleman, R., 1984. Subsidence and flexure along the Pratt-Welker seamount chain, *J. Geodyn.*, **1**, 29–60.
- Larson, R.L., 1991. Latest pulse of Earth—Evidence for a mid-cretaceous superplume, *Geology*, **19**, 547–550.
- Larson, R.L. & Erba, E., 1999. Onset of the mid-cretaceous greenhouse in the Barremanian-Aptian: Igneous events and the biological, sedimentary and geochemical responses, *Paleoceanography*, **14**, 663–678.
- Lincon, J.M., Pringle, M.S. & Silva, I.P., 1993. Mesozoic seafloor subsidence and the darwin rise, past and present, in *The Mesozoic Pacific: Geology, Tectonics, and Volcanism*, Vol. 77, pp. 279–305, eds Pringle, M.S., Sager, W.W., Sliter, W.V. & Stein, S., Geophysical Monographs, AGU.
- Lyons, S.N., Sandwell, D. & Smith, W.H.F., 2000. Three-dimensional estimation of elastic thickness under the Louisville Ridge, *J. geophys. Res.*, **105**(B6), 13 239–13 252.
- Maggi, A., Jackson, J.A., McKenzie, D. & Priestley, K., 2000. Earthquake focal depths, effective elastic thickness, and the strength of the continental lithosphere, *Geology*, **28**(6), 495–498.
- Mahoney, J.J. & Spencer, K.L., 1991. Isotopic evidence of the origin of the Manihiki and Ontong Java oceanic plateaus, *Earth planet. Sci. Lett.*, **104**, 196–210.
- Maia, M. & Hamed, J., 2002. The support mechanism of the young Foundation Seamounts inferred from bathymetry and gravity, *Geophys. J. Int.*, **149**(1), 190–210.
- Maia, M., Hemond, C. & Gente, P., 2001. Contrasted interactions between plume, upper mantle and lithosphere: foundation chain case, *Geochem. Geophys. Geosys.*, **2**, 2000GC000117.
- Mammerickx, J., 1992. The Foundation Seamounts—tectonic setting of a newly discovered seamount chain in the South-Pacific, *Earth planet. Sci. Lett.*, **113**(3), 293–306.
- Marks, K.M., 1996. Resolution of the Scripps/NOAA gravity field from satellite altimetry, *Geophys. Res. Lett.*, **23**(16), 2069–2072.
- Marks, K.M. & Sandwell, D.T., 1991. Analysis of geoid height versus topography for oceanic plateaus and swells using non-biased linear-regression, *J. geophys. Res.*, **96**(B5), 8045–8055.
- McKenzie, D., Jackson, J. & Priestley, K., 2005. Thermal structure of the oceanic and continental lithosphere, *Earth planet. Sci. Lett.*, **233**, 337–349.
- McNutt, M., 1998. Superswells, *Rev. Geophys.*, **36**, 211–244.
- McNutt, M.K., Winterer, E.L., Sager, W.W., Natland, J.H. & Ito, G., 1990. The Darwin Rise: a Cretaceous superswell? *Geophys. Res. Lett.*, **17**(8), 1101–1104.
- McNutt, M.K., Caress, D.W., Reynolds, J., Jordahl, K.A. & Duncan, R.A., 1997. Failure of plume theory to explain mid-plate volcanism in the southern Austral islands, *Nature*, **389**, 479–482.
- Menard, H.W., 1964. *Marine Geology of the Pacific*, McGraw-Hill, New York, pp. 271.
- Minshull, T.A. & Charvis, P., 2001. Ocean island densities and models of lithospheric flexure, *Geophys. J. Int.*, **145**(3), 731–739.
- Moore, J.G. & Clague, D.A., 1992. Volcano growth and evolution of the island of Hawaii, *Geol. Soc. Am. Bull.*, **104**(11), 1471–1484.
- Morgan, W., 1971. Convection plumes in the lower mantle, *Nature*, **230**, 42–43.
- Müller, R.D. & Roest, W.R., 1997. Digital isochrons of the world's ocean floor, *J. geophys. Res.*, **102**, 3211–3214.
- Nakanishi, M., Sager, W.W. & Klaus, A., 1999. Magnetic lineations within Shatsky Rise, northwest Pacific ocean: Implications for hot spot—triple junction interaction and oceanic plateau formations, *J. geophys. Res.*, **104**(B4), 7539–7556.
- Neuman, G.A., Forsyth, D. & Sandwell, D., 1993. Comparison of marine gravity from shipboard and high density satellite altimetry along the Mid Atlantic Ridge, *Geophys. Res. Lett.*, **20**(15), 1639–1642.

- Niu, Y.L. & Batiza, R., 1993. Chemical variation trends at fast and slow-spreading mid-ocean ridges, *J. geophys. Res.*, **98**(B5), 7887–7902.
- NOAA, 2003. GEODAS version 4.1, http://www.ngdc.noaa.gov/mgg/gdas/g4_sys.html.
- O'Connor, M., Stoffers, P.M. & Wijbrans, J.R., 1998. Migration rate of volcanism along the Foundation chain, SE Pacific, *Earth planet. Sci. Lett.*, **164**, 41–59.
- Parker, R.L., 1972. The rapid calculation of potential field anomalies, *Geophys. J. R. astr. Soc.*, **31**, 447–455.
- Parsons, B. & Sclater, J., 1977. An analysis of the variation of ocean floor bathymetry and heat flow with age, *J. geophys. Res.*, **82**, 803–827.
- Patriat, M. *et al.*, 2002. Deep crustal structure of the Tuamotu Plateau and Tahiti (French Polynesia) based on seismic refraction data, *Geophys. Res. Lett.*, **29**(14), art. no. 1656, doi:10.1029/2001GL013913.
- Pringle, M.S. & Dalrymple, G.B., 1993. Geochronological constraints on a possible hot-spot origin for Hess Rise and the Wentworth seamount chain, in *The Mesozoic Pacific: Geology, Tectonics, and Volcanism*, Vol. 77, pp. 263–277, eds Pringle, M.S., Sager, W.W., Sliter, W.V. & Stein, S., Geophysical Monographs, AGU.
- Rappaport, Y., Naar, D.F., Barton, C.C., Liu, Z.L. & Hey, R.N., 1997. Morphology and distribution of seamounts surrounding Easter Island, *J. geophys. Res.*, **102**, 24 713–24 728.
- Ribe, N.M., 1982. On the interpretation of frequency response functions for oceanic gravity and bathymetry, *Geophys. J. R. astr. Soc.*, **70**, 273–294.
- Ribe, N.M. & Watts, A.B., 1982. The distribution of intraplate volcanism in the Pacific Ocean basin: a spectral approach, *Geophys. J. R. astr. Soc.*, **71**, 333–362.
- Sager, W.W. & Han, H.-C., 1993. Rapid formation of the Shatsky Rise oceanic plateau inferred from its magnetic anomaly, *Nature*, **364**, 610–613.
- Sager, W.W. & Keating, B.H., 1984. Palaeomagnetism of Line Islands seamounts - Evidence for late Cretaceous and early Tertiary volcanism, *J. geophys. Res.*, **89**(B13), 1135–1151.
- Sager, W. & Pringle, M., 1987. Palaeomagnetic constraints on the origin and evolution of the Musicians and Southern Hawaiian Seamounts, central Pacific Ocean, in *Seamounts, Islands and Atolls Geophys. Mono. 43*, pp. 133–162, eds Keating, B.H., Fryer, P., Batiza, R. & Boehlert, G.W., American Geophysical Union, Washington DC.
- Sager, W.W., Kim, J., Klaus, A., Nakanishi, M. & Khankishieva, L.M., 1999. Bathymetry of the Shatsky Rise, northwest Pacific Ocean: Implications for oceanic plateau development at a triple junction, *J. geophys. Res.*, **104**(B4), 7557–7576.
- Sandwell, D., 1984. Thermo-mechanical evolution of oceanic fracture zones, *J. geophys. Res.*, **89**(B13), 11 401–11 413.
- Sandwell, D.T., Winterer, E.L., Mammerickx, J., Duncan, R.A., Lynch, M.A., Levitt, D.A. & Johnson, C.L., 1995. Evidence for diffuse extension of the Pacific plate from PukaPuka ridges and cross-grain gravity lineations, *J. geophys. Res.*, **100**, 15 087–15 099.
- Schlanger, S.O., Garcia, M.O., Keating, B.H., Naughton, J.J., Sager, W.W., Haggerty, J.A., Philpotts, J.A. & Duncan, R.A., 1984. Geology and geochronology of the Line Islands, *J. geophys. Res.*, **89**(13), 1261–1272.
- Schubert, G. & Sandwell, D., 1989. Crustal volumes of the continents and of oceanic and continental submarine plateaus, *Earth planet. Sci. Lett.*, **92**, 234–246.
- Schwank, D.C. & Lazarewicz, A.R., 1982. Estimation of seamount compensation using satellite altimetry, *Geophys. Res. Lett.*, **9**(8), 907–910.
- Sichoix, L., Bonneville, A. & McNutt, M.K., 1998. The seafloor swells and superswell in French Polynesia, *J. geophys. Res.*, **103**, 27 123–27 133.
- Sinton, C.W. & Duncan, R.A., 1997. Potential links between ocean plateau volcanism and global anoxia at the Cenomanian-Turonian boundary, *Economic Geology*, **92**, 836–842.
- Smith, D.K., 1988. Shape analysis of Pacific seamounts, *Earth planet. Sci. Lett.*, **90**, 457–466.
- Smith, W.H.F., 1990. Marine Geophysical Studies of Seamounts in the Pacific Ocean Basin, *PhD thesis*, Columbia Univ., 216 pp.
- Smith, W., 1993. On the accuracy of digital bathymetric data, *J. geophys. Res.*, **98**, 9591–9603.
- Smith, D.K. & Cann, J.R., 1992. The role of seamount volcanism in crustal construction at the Mid-Atlantic Ridge, *J. geophys. Res.*, **97**, 1645–1658.
- Smith, D.K. & Jordan, T.H., 1988. Seamount statistics in the Pacific Ocean, *J. geophys. Res.*, **93**, 2899–2918.
- Smith, W.H.F. & Sandwell, D.T., 1997. Global sea floor topography from satellite altimetry and ship depth soundings, *Science*, **277**, 1956–1962.
- Talandier, J. & Okal, E.A., 1987. Crustal structure in the Society and Tuamotu islands, *Geophys. J. R. astr. Soc.*, **88**, 499–528.
- Tarduno, J.A., Slitter, W.V., Leckie, L.K.M., Mayer, H., Mahoney, J.J., Musgrave, R., Storey, M. & Winterer, E.L., 1991. Rapid formation of Ontong Java Plateau by Aptian mantle plume volcanism, *Science*, **254**, 399–403.
- Ten Brink, U., 1991. Volcano spacing and plate rigidity, *Geology*, **19**, 397–400.
- Turcotte, D.L. & Schubert, G., 2002. *Geodynamics*, 2nd edn, Cambridge University Press, Cambridge.
- Turner, D.L., Jarrard, R.D. & Forbes, R.B., 1980. Geochronology and origin of the Pratt-Welker seamount chain, Gulf of Alaska: a new pole of rotation for the Pacific plate, *J. geophys. Res.*, **85**(B11), 6547–6556.
- Vallier, T.L., Dean, W.E., Rea, D.K. & Thiede, J., 1983. Geologic evolution of Hess Rise, central north Pacific-Ocean, *Geol. Soc. Am. Bull.*, **94**(11), 1289–1307.
- Vening Meinesz, F.A., 1941. Gravity over the Hawaiian Archipelago and over the Madeira area, *Proceedings of the Koninklijke Nederlandse Akademie van Wetenschappen*, **44**, 1–14.
- Verzhbitskii, E.V. & Merklin, L.R., 2000. Geothermal regime and origin of the Shatsky Rise, *Oceanology*, **40**(4), 583–589.
- Watts, A.B., 1978. An analysis of isostasy in the world's oceans 1. Hawaiian-Emperor seamount chain, *J. geophys. Res.*, **83**(B12), 5989–6004.
- Watts, A.B., 2001. *Isostasy and Flexure of the Lithosphere*, Cambridge University Press, Cambridge.
- Watts, A.B. & Burov, E., 2003. Lithospheric strength and its relationship to the elastic and seismogenic layer thickness, *Earth planet. Sci. Lett.*, **213**, 113–131.
- Watts, A.B. & Daly, S.F., 1981. Long wavelength gravity and topography anomalies, *Ann. Rev. Earth planet. Sci.*, **9**, 415–448.
- Watts, A.B. & Ribe, N.M., 1984. On geoid heights and flexure of the lithosphere at seamounts, *J. geophys. Res.*, **89**(B13), 11 152–11 170.
- Watts, A.B., Bodine, J.H. & Ribe, N.M., 1980. Observations of flexure and the geological evolution of the Pacific ocean basin, *Nature*, **283**, 532–537.
- Watts, A.B., Weissel, J.K., Duncan, R.A. & Larson, R.L., 1988. Origin of the Louisville Ridge and its relationship to the Eltanin fracture zone system, *J. geophys. Res.*, **93**(B4), 3051–3077.
- Watts, A.B., Sandwell, D., Smith, W.H.F. & Wessel, P., 2006. Global gravity, bathymetry, and the distribution of submarine volcanism through space and time, *J. geophys. Res.*, **111**, doi:10.1029/2005JB004083.
- Wessel, P., 1997. Sizes and ages of seamounts using remote sensing: implications for intraplate volcanism, *Science*, **277**, 802–805.
- Wessel, P., 2001. Global distribution of seamounts inferred from gridded Geosat/ERS-1 altimetry, *J. geophys. Res.*, **106**, 19 431–19 441.
- Wessel, P. & Lyons, S., 1997. Distribution of large Pacific seamounts from Geosat/ERS-1, *J. geophys. Res.*, **102**, 22 459–22 475.
- Wessel, P. & Smith, W.H.F., 1998. New, improved version of Generic Mapping Tools released, *EOS, Trans. Am. geophys. Un.*, **79**, 579.
- Wilson, J.T., 1963a. A possible origin of the Hawaiian islands, *Canadian Journal of Physics*, **41**, 863–870.
- Wilson, J.T., 1963b. Evidence from islands on the spreading of ocean floors, *Nature*, **197**, 536–538.
- Windom, K.E., Seifert, K.E. & Vallier, T.L., 1981. Igneous evolution of Hess Rise - Petrological evidence from DSDP leg 62, *J. geophys. Res.*, **86**(B7), 6311–6322.
- Woodhead, J.D., 1996. Extreme HIMU in an oceanic setting: The geochemistry of Mangaia Island (Polynesia), and the temporal evolution of the Cook-Austral hot spot, *J. Volc. Geotherm. Res.*, **72**, 1–19.

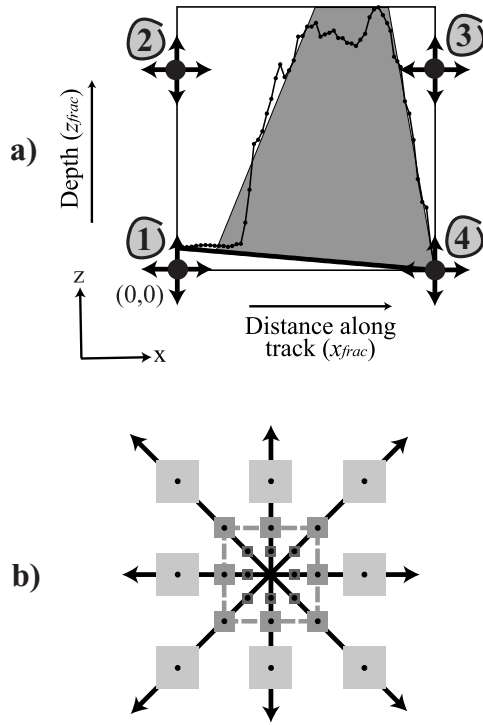


Figure A1. Search routine (a) ‘regional’ depth estimate by MiMIC passes under the seamount (bold line). Dots are data measured \sim every 1.5 km on cruise v3312. Distance and depths (x, z) are normalised to be between 0 and 1. From initial, or ‘seed’ points (numbered large black dots with arrows) the corners of the search-trapezium move, until they fit the bathymetry. The final best-fitting trapezium is shown in dark grey (Trapezium area = 105.057 per cent of the difference between the measured bathymetry and the regional bathymetry, misfit = 0.070696). (b) How the corners may move: 8 directions (arrows), larger step next time (lightest grey), same step (medium grey), and smaller step (darkest grey).

APPENDIX A: APPROXIMATING SEAMOUNTS AS TRAPEZIA

Fig. A1 illustrates a robust, scale-independent, automated method to approximate seamounts as trapezia using one of the bathymetric highs on cruise v3312 as an example.

To ensure scale invariance, the data are plotted in normalised distance, x_{frac} , and height, z_{frac} , which range from 0 to 1. $x_{frac} = \frac{(x-x_{start})}{(x_{finish}-x_{start})}$, and $z_{frac} = \frac{(z-z_{max})}{(z_{min}-z_{max})}$, where z_{min} and z_{max} are the shal-

lowest and deepest extremities of the seamount, whilst x_{start} and x_{finish} are the left and right hand limits, respectively.

The trapezium is described by the x and z coordinates of its 4 corners (x_{1-4}, z_{1-4}), numbered on Fig. A1(a). To efficiently invert for these 8 parameters a method is adopted where each of the corners of the moves sequentially (i.e. 1, 2, 3, 4, 1, 2 . . . etc) toward a trapezium that better fits the data. In a further simplex-like (Dantzig 1963) optimisation, each movement selects the best location from 8 directions, taking a step that is double, half, or the same size as last time (Fig. A1b) such that the movement possibilities for the next iteration upon that corner are increased in size, decreased, or remain the same, respectively. To simplify and stabilise the inversion the top is kept flat and the corners are required to retain their relative position (e.g. corner 2, upper-left).

Data is resampled at equal intervals *along the line* between points so the visual shape is fitted unaffected by seafloor slope and data density.

Total misfit, Δ_{tot} , is an equally-weighted sum of misfits, Δ_{side} , for the 4 sides of the trapezium. Each $\Delta_{side} = \frac{\sum |measured - line|}{n}$, where n is the number of data points (n kept ≥ 1). Misfits for the left side are horizontal, calculated for points with $z_{frac} < z_2$ to the left of the summit. The right side mirrors this using $z_{frac} < z_3$. Misfit for the top is vertical and calculated for the remainder of the points. Basal misfit is vertical and between the bottom and regional depth.

Initial locations of the corners used are (0, 0) (0, 0.75) (1, 0.75) (1, 0), and initial step size is 0.1. Iteration is stopped after 20 cycles, when all points are not moving (i.e. step to use is < 0.001), or $\Delta_{tot} < 0.01$. Commonly, 8–12 iterations are required, and the 340 seamounts of v3312 (Fig. A2) are approximated in 45 seconds by an ~ 1 GHz processor, about 0.13 s per fit.

APPENDIX B: VALUE OF PHYSICAL PROPERTIES

From drilling (Hyndman *et al.* 1979) seamount density, ρ_{load} , is commonly stated as 2800 kg m^{-3} (e.g. Freedman & Parsons 1986; Craig & Sandwell 1988; Schubert & Sandwell 1989; Wessel & Lyons 1997), comparable to average oceanic basement ($2860 \pm 30 \text{ kg m}^{-3}$) (Carlson & Herrick 1990). However, $2950 \text{ kg m}^{-3} > \rho_{load} \geq 2100 \text{ kg m}^{-3}$, probably dependent upon the amount of extrusives present and the extent of mass wasting (Carlson & Herrick 1990; Hammer *et al.* 1994; Minshull & Charvis 2001; Turcotte & Schubert 2002). Poisson’s ratio (ν) is 0.25–0.5 (e.g. Calmant *et al.* 1990; Ribe & Watts 1982; Freedman & Parsons 1986; Craig & Sandwell 1988), and Young’s modulus (E) is $6.5 \times 10^{10} \text{ N m}^{-1}$ (e.g. Sandwell 1984; Craig & Sandwell 1988) to 10^{12} N m^{-1} (Calmant *et al.* 1990).

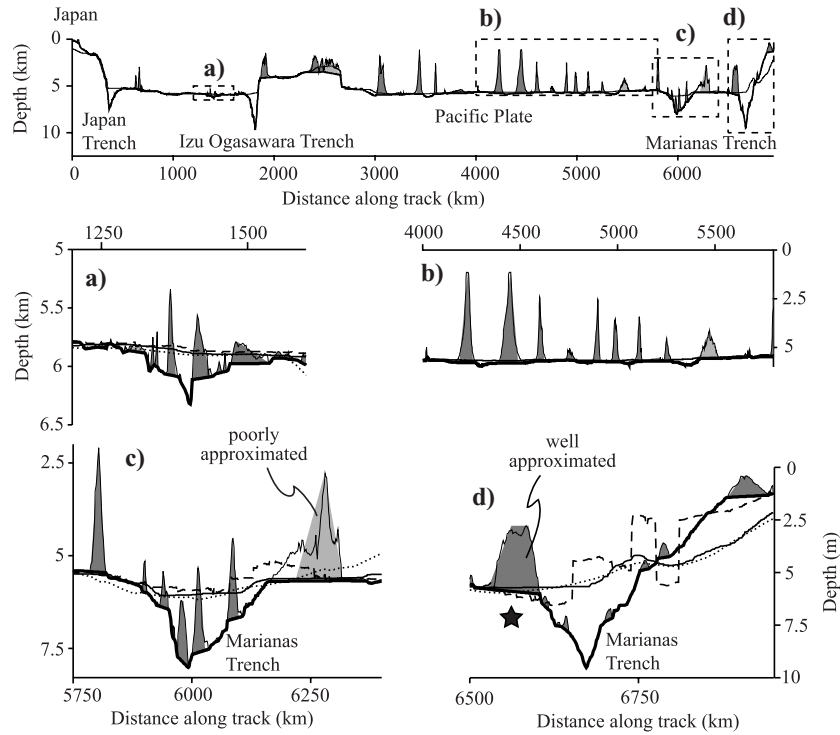


Figure A2. Isolation (by **MiMIC**) and approximation (as trapezia) of seamounts for bathymetry data collected on cruise v3312. Expanded sections are marked by dashed boxes and labelled with letters a–d. In these, well-fitted seamounts are dark-grey, poorly fitted highs light-grey. Feint line is bathymetry, bold line is the ‘regional’ depth (i.e. that which passes underneath seamounts) estimated by **MiMIC**, and for comparison intermediate thickness solid, dotted and dashed lines are regional depths estimated by spatial median, mean and mode, respectively (400 km wide, filter1d of GMT Wessel & Smith (1998)). **MiMIC** is applied exactly as first pass in Hillier & Watts (2004, 2005a). Star indicates seamount in Fig A1.